REVISION 2

# Synthesis of K-dominant tourmaline

Eleanor Berryman[1,*], Bernd Wunder[2] and Dieter Rhede[2]

[1]Fachgebiet Mineralogie-Petrologie, Technische Universität Berlin, 13355 Berlin, Germany.

[2]GeoForschungsZentrum Potsdam, 14473 Potsdam, Germany.

*E-mail: berryman.eleanor@gmail.com

## Abstract

K-dominant tourmaline was synthesized in the system $MgO$-$Al_2O_3$-$B_2O_3$-$SiO_2$-$KCl$-$H_2O$ at 700 °C and 4.0 GPa. The crystals were zoned and characterized by less-potassic cores (1.46 wt% $K_2O$) and more-potassic rims (up to 3.44 wt% $K_2O$). The K-dominant tourmaline rims are represented by the average structural formula $(K_{0.64(3)}\square_{0.36(3)})(Mg_{2.60(7)}Al_{0.40(7)})(Al_{5.97(3)}Si_{0.03(3)})(Si_{5.99(1)}Al_{0.01(1)})(BO_3)_3(OH)_{3.92(8)}O_{0.08(8)}$, which is analogous to the structural formula of dravite and is referred to here as "K-dravite"; the maximum K content (3.44 wt% $K_2O$) represents occupancy of the X site by 0.71 K pfu. The addition of Na to the system in approximately equal molar proportions to K results in the crystallization of K-bearing, Na-rich dravitic tourmaline, dramatically reducing the K content to an average value of 0.47 wt% $K_2O$, corresponding to 0.10 K pfu. This suggests that a K-dominated bulk composition is necessary for K-dominant tourmaline crystallization. Compositional zoning shows that solid solution exists between end-member compositions of "K-dravite" [$(KMg_3Al_6Si_6O_{18}(BO_3)_3(OH)_3(OH)$] and dravite via the isovalent exchange ${}^{X}K({}^{X}Na)_{-1}$, magnesio-foitite via the coupled substitution ${}^{X}K^{Y}Mg({}^{X-Y}Al)_{-1}$, and "K-olenite" via the coupled

substitution $^{Y}MgOH(^{Y}AlO)_{-1}$. Structural refinement of the powder X-ray data provides a unit-cell volume for the synthesized "K-dravite" of 1580.1(5) Å$^3$, which is greater than that determined for K-bearing dravitic tourmaline synthesized at the same conditions (1574.9(4) Å$^3$). We interpret this to reflect expansion of the crystal structure due to incorporation of the relatively large $K^+$ ion.

Keywords: tourmaline, potassium end-member, high pressure, synthesis, Na-K solid solution

## Introduction

Tourmaline, with the general formula $^{[9]}X^{[6]}Y_3{}^{[6]}Z_6{}^{[4]}T_6O_{18}(^{[3]}BO_3)_3V_3W$ (Hawthorne and Henry 1999; Hamburger and Buerger 1948), is known for its ability to incorporate a wide range of elements, resulting in the 28 different end-members currently accepted by the International Mineralogical Association's Commission on New Minerals, Nomenclature and Classification (IMA-CNMNC) and additional end-members continuously being discovered (e.g., London et al. 2006; Wodara and Schreyer 2001; Selway et al. 1998). The tourmaline supergroup has been subdivided into three primary types based on the dominant occupancy of the X-site: the alkali-, calcic-, and X-vacant ($^{-}$) tourmaline groups (Henry et al. 2011). The alkali-tourmaline group includes tourmalines which have $(Na^+ + K^+) > Ca^{2+}$ and $(Na^+ + K^+) > {}^{-}$ at their X-site (Henry et al. 2011). Even though K-dominant tourmaline has been found in nature (e.g., "K-oxy-dravite" with 2.75 wt% $K_2O$ or 0.576 K pfu by Shimizu and Ogasawara (2005, 2013), and "K-povondraite" with 2.2 wt% $K_2O$ or 0.56 K pfu by Grice et al. (1993) or 0.60 K pfu by Žáček et al. (2000)), its rarity has precluded it from being recognized as a distinct end-member, and only Na, Ca, and X-vacant end-members are currently defined. In addition, $K^+$ is typically considered incompatible in tourmaline, likely because of its large ionic radius (1.55 Å in nine-fold

coordination), which is 25% larger than $Na^+$ (1.24 Å in nine-fold coordination) (Shannon 1976). However, the occurrence of micro-diamond inclusions in "K-oxy-dravite" from the Kokchetav Massif, Kazakhstan, raised the question of whether K is incorporated more readily at high pressure (Shimizu and Ogasawara 2005, 2013; Ota et al. 2008), or in the presence of K-rich fluids (Marschall et al. 2009). We report here the first synthesis of "K-dravite", which forms a solid-solution with the Na-bearing end-member dravite [$NaMg_3Al_6Si_6O_{18}(BO_3)_3(OH)_3OH$] via $^{X}K^{X}Na_{-1}$ exchange.

## Experimental details

K-bearing tourmaline was synthesized at 4.0 GPa and 700 °C after 4 days using an end-loaded piston-cylinder press. A mixture of solid MgO, γ-$Al_2O_3$, $SiO_2$, and $H_3BO_3$ in the atomic proportions of end-member dravite with 20-mol% excess $SiO_2$ and 100-mol% excess $H_3BO_3$ to facilitate tourmaline crystallization (Werding and Schreyer 1984) was ground for two hours. Prior to being weighed, MgO and γ-$Al_2O_3$ were dried at 400 °C for 1 day to reverse any hydration or carbonatization that may have occurred during storage. Two experiments were prepared using clean gold capsules (10-mm length, 3-mm outer diameter, 0.25-mm wall thickness) that had been fired at 600 °C for 2 days. The capsule for run #EB1 was filled with 10.81 mg of the solid mixture and 3.39 mg of a KCl-saturated solution (3.85 *M* KCl), and the capsule for run #EB2 with 10.87 mg of the solid mixture, 2.58 mg of a 3.85-*M* KCl solution, and 2.08 mg of a 5-*M* NaCl solution. The capsules were welded shut, reweighed after being left in an oven at 100 °C overnight to ensure a good seal, and placed together in a steel furnace assembly with sodium chloride as a pressure medium. Pressure was calibrated according to the quartz-coesite transition (Mirwald and Massonne 1980), which is accurate within 50 MPa. Temperature was measured with a Ni-CrNi thermocouple placed into the assembly close to the center of the

two capsules; its error is estimated to be ± 10 °C. Once pressure was stable at 4.0 GPa, the system was heated to 700 °C within 30 minutes and left for 4 days. Pressure was maintained within 50 MPa throughout the duration of the experiment. At the end of the experiment, the samples were quenched isobarically to a temperature below 200 °C in less than 15 seconds prior to the slow release of pressure. Once removed from the assembly, the capsules were cleaned and reweighed to check for leakage. Finally, the sample material was carefully removed and prepared for analysis by optical microscopy, electron microprobe (EMP) and X-ray diffraction (XRD).

## Chemical Analysis

EMP-analyses were done on the epoxy-mounted, polished, and carbon-coated samples using a JEOL Hyperprobe JXA-8500F equipped with a thermal field-emission cathode and five wavelength-dispersive spectrometers operated with a 8.0-kV accelerating voltage, a 10-nA beam current, and a 1–5-μm beam diameter. Signals for all elements were counted for 20 s, except for Na, which had a 10-s counting time. The standards used were orthoclase (K, Si, and Al), jadeite (Na), and periclase (Mg). Data reduction was done using a $\varphi(\rho Z)$ correction scheme (CITZAF; Armstrong 1995). Under these conditions, analytical errors and detection limits ($1\sigma$) are 0.98% and 280 ppm for Si, 0.63% and 205 ppm for Al, 1.18% and 189 ppm for Mg, 4.82% and 251 ppm for Na and 13.19% and 383 ppm for K, respectively. Wavelength-dispersive element X-ray maps were obtained using a moving-stage program with an 8.0-kV accelerating voltage, a 10-nA beam current, and a 0.10-μm step interval. The counting time per step was 250 ms for element X-ray maps of tourmaline synthesized in the presence of a KCl fluid (#EB1, Fig. 1) and 300 ms for those synthesized in the presence of a KCl-NaCl fluid (#EB2, Fig. 2). The X-ray intensities

were measured for K, Mg, Al, and Si in both samples and, in the case of #EB2, additionally for Na and plotted on separate element maps based on a color scale.

## X-ray crystallography

Powder-XRD patterns for both samples were recorded on a STOE Stadi P diffractometer equipped with a position-sensitive detector (PSD) using Cu $K\alpha_1$ X-radiation measured in the 5–125° 2θ range, generated with a 40-kV accelerating voltage, a 40-mA beam current, and a germanium (*111*) primary monochromator. Cell dimensions were determined by Rietveld refinement using the GSAS software package (Larson and Von Dreele 1987). Initial structure models for tourmaline (dravite), coesite, santite, and sylvite applied the structural parameters of Buerger et al. (1962), Geisinger et al. (1987), Zachariasen and Plettinger (1963), and Barrett and Wallace (1954), respectively. In the tourmaline structure-refinement, average site-occupancy values as determined by EMP were used.

## Results and discussion

The experiments produced a product assemblage of tourmaline, coesite, and, in the Na-free system, santite ($KB_5O_8{\cdot}4H_2O$) and sylvite. The synthesized tourmaline crystals were on average 10 μm long and 1–2 μm wide, but ones up to 50 μm long were observed. Tourmaline synthesized in the presence of a KCl fluid (#EB1) had the highest K content, with up to 3.44 wt% $K_2O$ measured with a 5-μm beam. As shown in Fig. 1, crystals were compositionally zoned, the darker cores being less potassic than the brighter rims (Table 1). The crystal cores have the lowest concentration of K (1.46 wt% $K_2O$, 0.30 K pfu), whereas the rims have up to 3.44 wt% $K_2O$ (0.71 K pfu), thereby forming K-dominant tourmaline. This zoning correlates with increasing Mg and decreasing Al incorporation with crystal growth. As a result, we interpret the

increased K incorporation towards the rims to reflect the coupled substitution $^{X}K^{+} + {}^{Y}Mg^{2+} = {}^{X\square} + {}^{Y}Al^{3+}$, discussed in greater detail below. Although the solution was saturated with respect to KCl at atmospheric conditions, it was undersaturated at the experimental conditions. It is thus likely that even greater K incorporation could occur with a more KCl-concentrated solution. The addition of aqueous NaCl to the fluid (#EB2) reduced the concentration of KCl by 45%, from 3.85 *M* to 2.13 *M*. However, the proportion of K incorporated at the X-site decreased by far more than 45%, down to 0.10 K pfu (Table 1). Even though this is still relatively K-rich compared to tourmaline typically found in nature, the dominant occupancy of the X-site by Na indicates that K-rich dravite was synthesized. The effect of varying fluid composition indicates that bulk composition has a significant control on the crystallization of "K-dravite" and that a K-dominant and Na-poor fluid is required for its crystallization.

The EMP data were normalized to 15 cations at the Y, Z, and T sites (15 YZT) and alternatively to 24.5 O (the number of oxygen atoms in tourmaline's structure not associated with B or H, assuming a structure with 4 OH), assuming 3 B pfu in both cases (Table 1). Both normalizations assume the absence of B at the T site ($^{[4]}B$), which, however, cannot be excluded. The two normalization schemes are in good agreement, with discrepancies only in terms of the W site. Although normalization to 15 YZT is normally favored because it permits the relative occupancy of $O^{2-}$ and $OH^{-}$ in the W site to be calculated, in the case of the "K-dravite" cores (#EB1), an insufficient amount of positive charge among the cations results in the W site being underfilled (Table 1; Fig. 3b). This is best explained by the initial crystallization of tourmaline being nonstoichiometric, as observed in earlier tourmaline-synthesis experiments (e.g., von Goerne et al. 1999), or by inaccuracy in the EMP measurements arising from porosity between abundant crystal nuclei in the cores.

133 The "K-dravite" end-member formula is $KMg_3Al_6Si_6O_{18}(BO_3)_3(OH)_3(OH)$ and is related
134 to end-member dravite $[NaMg_3Al_6Si_6O_{18}(BO_3)_3(OH)_3(OH)]$ by isovalent substitution at the X
135 site: $K^+ \Leftrightarrow Na^+$, i.e. the exchange vector ${}^{X}K({}^{X}Na)_{-1}$ (Fig. 4). Shimizu and Ogasawara (2005)
136 noted this exchange in describing their K-rich tourmaline from the Kokchetav Massif in
137 Kazakhstan as ranging from 0.11 to 0.55 $X_{K\text{-oxy-dravite}}$ and again when they showed that their most
138 K-rich tourmaline was a continuous solid-solution with Ca-, Na- and $^{\square}$-tourmaline (Shimizu and
139 Ogasawara 2013). However, whereas they propose an end-member analogous to oxy-dravite
140 $[Na(Mg_2Al)Al_6Si_6O_{18}(BO_3)_3(OH)_3O]$, our synthetic K-tourmaline with ${}^{Y}Al<1$ (Table 1) is
141 analogous to dravite, as predicted by Henry et al. (2011). Furthermore, the compositional zoning
142 of the synthesized "K-dravite" indicates that there is solid solution between the end-member
143 compositions of "K-dravite" and X-site-vacant tourmaline, magnesio-foitite
144 $[^{\square}(Mg_2Al)Al_6Si_6O_{18}(BO_3)_3(OH)_3(OH)]$, via the coupled substitution ${}^{X}K^+ + {}^{Y}Mg^{2+} = {}^{X\square} + {}^{Y}Al^{3+}$
145 (exchange vector ${}^{X}K{}^{Y}Mg({}^{X\square}{}^{Y}Al)_{-1}$; Fig. 3a), and, to a lesser extent, between the end-member
146 compositions of "K-dravite" and the K analogue of the Al-tourmaline, olenite
147 $[KAl_3Al_6Si_6O_{18}(BO_3)_3O_3(OH)]$, via the coupled substitution ${}^{Y}Mg^{2+} + (OH)^- = {}^{Y}Al^{3+} + O^{2-}$
148 (exchange vector ${}^{Y}MgOH({}^{Y}AlO)_{-1}$; Fig. 3b). Element X-ray mapping of radiating crystal clusters
149 (Figs. 1 and 2) illustrates these solid solutions, particularly that with magnesio-foitite; concurrent
150 with the increase in K (or Na in the sodium-bearing system), the Mg content is increased and Al
151 content decreased in the crystal rims. In the case of the K-rich dravitic tourmaline crystals
152 (#EB2), Mg and, to a lesser extent, K are also enriched in the crystal rim (Fig. 2). Concurrently,
153 Na and Si also show increasing concentration with crystal growth. The increasing incorporation
154 of Na in K-rich dravite (#EB2) is similar in behavior to the incorporation of K in "K-dravite"
155 from #EB1. However, whereas Na steadily increases in concentration, the ratio of K to vacancies

156 remains relatively constant at 1:4 (dashed line in Fig. 4). The increased incorporation of Si is
157 complementary to the decreasing Al content, based on the coupled substitution $^{Y}Al^{3+} + {}^{T}Al^{3+} =$
158 $^{Y}Mg^{2+} + {}^{T}Si^{4+}$ (exchange vector $^{Y}Mg^{T}Si(^{Y}Al^{T}Al)_{-1}$). The favoring of the early crystallization of
159 Al-rich tourmaline in the crystal cores is attributed to the lower mobility of Al in the fluid and,
160 along with increasing Mg content, is consistent with earlier tourmaline-synthesis experiments
161 (e.g., von Goerne et al. 1999). Increasing Si content with crystal growth is also observed in the
162 "K-dravite", but is overshadowed by the solid solution with magnesio-foitite described above
163 (Fig. 1).

164 Details and results of the Rietveld refinements of powder-XRD spectra from both
165 experiments are given in Table 2. The relatively high sigma values result from the
166 inhomogeneity of the synthesized tourmaline. Nonetheless, taken qualitatively, the unit-cell
167 volumes of tourmaline synthesized in both experiments is smaller than that of end-member
168 dravite (1595.1 $Å^3$; Buerger et al. 1962). This is likely caused by significant vacancies at the X-
169 site (Table 1). Furthermore, the larger unit-cell volume of the synthetic "K-dravite" (#EB1)
170 likely reflects the increased incorporation of the relatively large $K^+$ ion at the X-site compared to
171 synthetic K-bearing dravite (#EB2). Ertl et al. (2008) showed that $^{[4]}B$ content in Al-rich
172 tourmaline is related to the unit-cell volume. Based on this relation, a unit-cell volume less than
173 1539.3 $Å^3$ is necessary to indicate significant incorporation of B at the T site (Ertl et al. 2008).
174 The unit-cell volume of tourmaline synthesized in both experiments is significantly larger than
175 this value, supporting the assumption of no $^{[4]}B$ in the normalization procedure (Table 2).

176 Two preliminary multi-anvil experiments with bulk compositions identical to #EB1 were
177 done at 700 °C and 6 and 8 GPa, respectively, to investigate the upper-pressure stability of "K-
178 dravite". The experiments yielded mainly a combination of boro-muscovite and phengite, but no

tourmaline. These results suggest that the upper stability of "K-dravite" is between 4.0 GPa and 6.0 GPa, consistent with the stability of dravite in a silica-saturated system (4.5–5.0 GPa at 700 °C; Ota et al. 2008).

## Implications

Although $K^+$ is approximately 25% larger than $Na^+$ (Shannon 1976), the tourmaline structure is able to incorporate K at the X site given the appropriate environment. Based on our synthesis experiments, high pressure and a fluid with at least 3.85 *M* K is required to incorporate significant amounts of K. However, additional experiments are needed to determine the minimum pressure required for the synthesis of K-dominant tourmaline. Although tourmaline still incorporates K in the presence of Na, the tourmaline structure preferentially incorporates the smaller Na ion. As a result, K incorporation is expected to be more prominent in Na-poor and probably Ca-poor environments.

Moreover, the alkali-tourmaline group can be subdivided to include both Na and K end-member tourmaline. Although the K-dominant tourmaline synthesized here is analogous to dravite, its solid solution with the Al-end-member olenite (Fig. 3b) suggests that a K-dominant olenite [$KAl_3Al_6Si_6O_{18}(BO_3)_3O_3(OH)$], namely "K-olenite", may also exist. However, additional experiments are required to confirm its stability.

## Acknowledgements

The authors thank H.-P. Nabein for generating the XRD patterns and U. Dittmann for sample preparation. The authors are indebted to G. Franz and W. Heinrich for sharing ideas, insightful discussion and critical reading of earlier versions of the manuscript. Thoughtful reviews by H. Marschall, F.C. Hawthorne, and R. Shimizu improved the final version of the manuscript. This

201 study was financially supported by funding from the DFG granted to G. Franz and W. Heinrich
202 (FR 557/ 31-1; HE 2015/16-1). E.B. is grateful for a scholarship awarded by NSERC.

203 References

204 Armstrong, J.T. (1995) CITZAF: a package of correction programs for the quantitative electron
205 microbeam X-ray-analysis of thick polished materials, thin films, and particles. Microbeam
206 Analysis, 4, 177-200.

207 Barrett, W.T., and Wallace, W.E. (1954) Studies of NaCl-KCl solid solutions. I. Heats of
208 formation, lattice spacings, densities, Schottky defects and mutual solubilities. Journal of
209 the American Chemical Society, 76, 366-369.

210 Buerger, M.J., Burnham, C.W., and Peacor, D.R. (1962) Assessment of the several structures
211 proposed for tourmaline. Acta Crystallographica, 15, 583-590.

212 Ertl, A., Tillmanns, E., Ntaflos, T., Francis, C., Giester, G., Körner, W., Hughes, J.M., Lengauer,
213 C., and Prem, M. (2008) Tetrahedrally coordinated boron in Al-rich tourmaline and its
214 relationship to the pressure-temperature conditions of formation. European Journal of
215 Mineralogy, 20, 881-888.

216 Geisinger, K.L., Spackman, M.A., and Gibbs, G.V. (1987) Exploration of structure, electron
217 density distribution, and bonding in coesite with fourier and pseudoatom refinement
218 methods using single-crystal X-ray diffraction. Journal of Physical Chemistry, 91, 3237-
219 3244.

220 Grice, J.D., Ercit, T.S., and Hawthorne, F.C. (1993) Povondraite, a redefinition of the tourmaline
221 ferridravite. American Mineralogist, 78, 433-436.

222 Hamburger, G.E., and Buerger, M.J. (1948) The structure of tourmaline. American Mineralogist,
223 33, 532-540.

224 Hawthorne, F.C., and Henry, D.J. (1999) Classification of the minerals of the tourmaline group.
225 European Journal of Mineralogy, 11, 201-215.

226 Henry, D.J., Novák, M., Hawthorne, F.C., Ertl, A., Dutrow, B.L., Uher, P., and Pezzotta, F.
227 (2011) Nomenclature of the tourmaline-supergroup minerals. American Mineralogist, 96,
228 895-913.

229 Larson, A.C., and Von Dreele, R.B. (1987) Generalized structure analysis system. Los Alamos
230 National Laboratory Report LA-UR-86-748.

231 London, D., Ertl, A., Hughes, J.M., Morgan VI, G.B., Fritz, E.A., and Harms, B.S. (2006)
232 Synthetic Ag-rich tourmaline: Structure and chemistry. American Mineralogist, 91, 680-
233 684.

234 Marschall, H.R., Korsakov, A.V., Luvizotto, G.L., Nasdala, L., and Ludwig, T. (2009) On the
235 occurrence and boron isotopic composition of tourmaline in (ultra)high-pressure
236 metamorphic rocks. Journal of the Geological Society, London, 166, 811-823.

237 Mirwald, P.W., and Massonne, H.-J. (1980) Quartz-coesite transition and the comparative
238 friction measurements in piston-cylinder apparatus using talc-alsimag-glass (TAG) and
239 NaCl high pressure cells: A discussion. Neues Jahrbuch für Mineralogie, 1980, 469-477.

240 Ota, T., Kobayashi, K. Katsura, T., and Nakamura, E. (2008) Tourmaline breakdown in a pelitic
241 system: implications for boron cycling through subduction zones. Contributions to
242 Mineralogy and Petrology, 155, 19-32.

243 Selway, J.B., Novák, M., Hawthorne, F.C., Černý, P., Ottolini, L., and Kurtis Kyser, T. (1998)
244 Rossmanite, $\square(LiAl_2)Al_6(Si_6O_{18})(BO_3)_3(OH)_4$, a new alkali-deficient tourmaline:
245 Description and crystal structure. American Mineralogist, 83, 896-900.

246 Shannon, R.D. (1976) Revised Effective Ionic Radii and Systematic Studies of Interatomic
247 Distances in Halides and Chalcogenides. Acta Crystallographica, A 32, 751.

248 Shimizu, R., and Ogasawara, Y. (2005) Discovery of K-tourmaline in diamond-bearing quartz-
249 rich rock from the Kokchetav Massif, Kazakhstan. Mitteilungen der Österreichischen
250 Mineralogischen Gesellschaft, 150, 141.

251 --- (2013) Diversity of potassium-bearing tourmalines in diamondiferous Kokchetav UHP
252 metamorphic rocks: A geochemical recorder from peak to retrograde metamorphic stages.
253 Journal of Asian Earth Sciences, 63, 39-55.

254 Von Goerne, G., Franz, G., and Wirth, R. (1999) Hydrothermal synthesis of large dravite crystals
255 by the chamber method. European Journal of Mineralogy, 11, 1061-1077.

256 Werding, G., and Schreyer, W. (1984) Alkali-free tourmaline in the system $MgO$-$Al_2O_3$-$B_2O_3$-
257 $SiO_2$-$H_2O$. Geochimica et Cosmochimica Acta, 48, 1331-1344.

258 Wodara, U., and Schreyer, W. (2001) X-site vacant Al-tourmaline: a new synthetic end-member.
259 European Journal of Mineralogy, 13, 521-532.

260 Zachariasen, W.H., and Plettinger, H.A. (1963) Refinement of the structure of potassium
261 pentaborate tetrahydrate. Acta Crystallographica, 16, 376-379.

Žáček, V., Jiří, F., Petrov, A., and Hyršl, J. (2000) Tourmalines of the povondraite-(oxy)dravite series from the cap rock of meta-evaporite in Alto Chapare, Cochabamba, Bolivia. Journal of the Czech Geological Society, 45, 3-12.

Figure 1. Back-scattered-electron image (top right) and EMP wavelength-dispersive element X-ray maps of tourmaline synthesized in the presence of a KCl fluid after 4 days at 700 °C and 4.0 GPa (#EB1). The colour scale to the left of each element X-ray map ranges from black to red, representing low to high number of counts, respectively.

Figure 2. Back-scattered-electron image (top right) and EMP wavelength-dispersive element X-ray maps of tourmaline synthesized in the presence of a KCl-NaCl fluid after 4 days at 700 °C and 4.0 GPa (#EB2). The colour scale to the left of each element X-ray map ranges from black to red, representing low to high number of counts, respectively

Figure 3. EMP-analyses of compositional zoning in tourmaline, with growth direction indicated by arrows; (a) from #EB1 (circles) and #EB2 (triangles) representing solid solution between end-member magnesio-foitite [$\square Mg_2Al)Al_6Si_6O_{18}(BO_3)_3O_3(OH)$] and end-member "K-dravite" [$KMg_3Al_6Si_6O_{18}(BO_3)_3(OH)_3(OH)$] via the exchange vector ${}^{X}K{}^{Y}Mg({}^{X}\square{}^{Y}Al)_{-1}$, or end-member dravite [$NaMg_3Al_6Si_6O_{18}(BO_3)_3(OH)_3(OH)$] via the analogous exchange vector ${}^{X}Na{}^{Y}Mg({}^{X}\square{}^{Y}Al)_{-1}$; (b) from #EB1 representing a solid solution between end-member "K-dravite" and end-member "K-olenite" [$KAl_3Al_6Si_6O_{18}(BO_3)_3O_3(OH)$] via the exchange vector ${}^{Y}MgOH({}^{Y}AlO)_{-1}$.

Figure 4. Ternary diagram of the occupancy of the X-site for tourmaline formed in the presence of a KCl fluid (circles, #EB1) and in the presence of a KCl-NaCl fluid (triangles, #EB2). The dashed line indicates values of variable Na content with a ratio of 1K:4$^{-}$ (X-vacant). Arrows indicate the direction of crystal growth.

Table 1. Composition (EMP-analyses) and stoichiometry of synthesized tourmaline normalized to 15 YZT and 24.5 O pfu

| oxide (wt%) | | 100 mol% KCl | | | | 49 mol% KCl, 51mol% NaCl | |
|---|---|---|---|---|---|---|---|
| | | rims | | cores | | | |
| | | *n* = 10 | | *n* = 24 | | *n* = 16 | |
| $K_2O$ | | 3.13(14) | | 1.46(53) | | 0.47(15) | |
| $Na_2O$ | | 0.02(2) | | 0.03(3) | | 1.66(35) | |
| MgO | | 10.89(31) | | 10.24(57) | | 9.88(89) | |
| $Al_2O_3$ | | 33.85(41) | | 35.40(94) | | 36.32(158) | |
| $SiO_2$ | | 37.64(40) | | 36.49(100) | | 35.47(93) | |
| Total | | 85.52(57) | | 83.61(99) | | 83.80(81) | |
| **Normalization** | | **15 YZT** | **24.5 O** | **15 YZT** | **24.5 O** | **15 YZT** | **24.5 O** |
| X | K | 0.64(3) | 0.64(3) | 0.30(11) | 0.30(11) | 0.10(3) | 0.10(3) |
| | Na | 0.00(1) | 0.00(1) | 0.01(1) | 0.01(1) | 0.52(11) | 0.52(11) |
| | □ | 0.36(3) | 0.36(3) | 0.69(11) | 0.69(11) | 0.38(9) | 0.38(9) |
| $Y_3$ | Mg | 2.60(7) | 2.59(8) | 2.45(13) | 2.46(14) | 2.38(21) | 2.38(21) |
| | Al | 0.40(7) | 0.41(8) | 0.55(13) | 0.54(14) | 0.62(21) | 0.62(21) |
| $Z_6$ | Al | 5.97(3) | 5.96(4) | 6.00(2) | 6.00(2) | 6.00(0) | 6.00(0) |
| | Si | 0.03(3) | 0.02(2) | 0.00(2) | 0.09(8) | 0.00(0) | 0.01(4) |
| $T_6$ | Si | 5.99(1) | 5.99(1) | 5.85(14) | 5.80(18) | 5.72(13) | 5.71(14) |
| | Al | 0.01(1) | 0.01(1) | 0.15(14) | 0.20(18) | 0.28(13) | 0.29(14) |
| $(BO_3)_3$ | B | 3.00[a] | 3.00[a] | 3.00[a] | 3.00[a] | 3.00[a] | 3.00[a] |
| $V_3$ | OH | 3.00(0) | 3.00[a] | 3.00(0) | 3.00[a] | 3.00(0) | 3.00[a] |
| W | OH | 0.92(8) | 1.00[a] | 0.69(23) | 1.00[a] | 0.90(9) | 1.00[a] |
| | O | 0.08(8) | 0[a] | 0.01(4) | 0[a] | 0.03(5) | 0[a] |

Note: [a] Values fixed during normalization. n is the number of analyses.

287

Table 2. Unit-cell parameters of synthesized tourmaline

| | | | |
|---|---|---|---|
| Refinement details | Experiment | #EB1 | #EB2 |
| | $\chi^2$ | 2.01 | 1.63 |
| | DWd | 1.03 | 1.27 |
| Phase proportions | Tourmaline | 78 wt% | 86 wt% |
| | Coesite | 10 wt% | 14 wt% |
| | Santite | 11 wt% | n/a |
| | Sylvite | <1 wt% | n/a |
| Unit-cell parameters | $a = b$ | 15.927(2) Å | 15.913(1) Å |
| | $c$ | 7.193(1) Å | 7.181(1) Å |
| | $V$ | 1580.1(5) Å$^3$ | 1574.9(4) Å$^3$ |

Note: DWd indicates the Durbin-Watson statistic for the refinement. Phase proportions are approximate values (± 2 wt%).

288

CROP: FIGURE 1

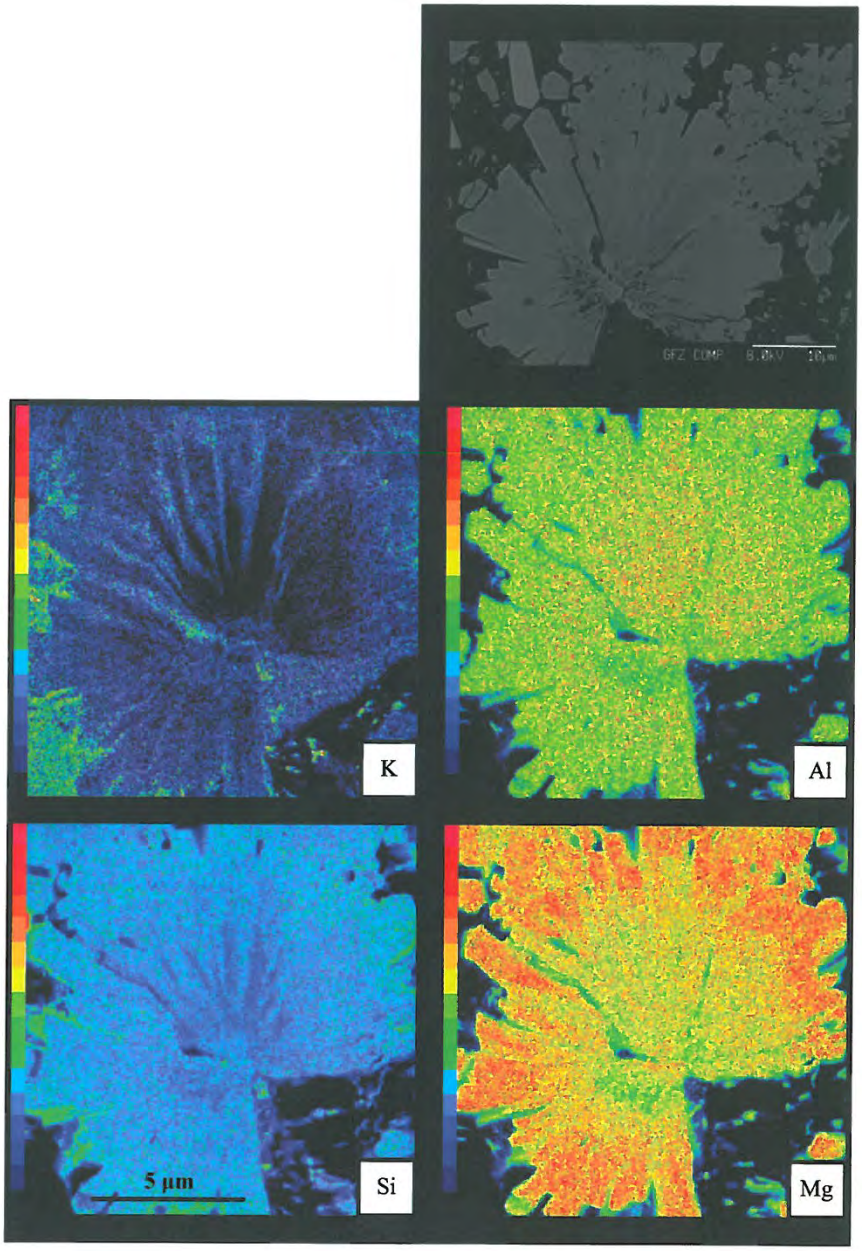

CROP: FIGURE 2

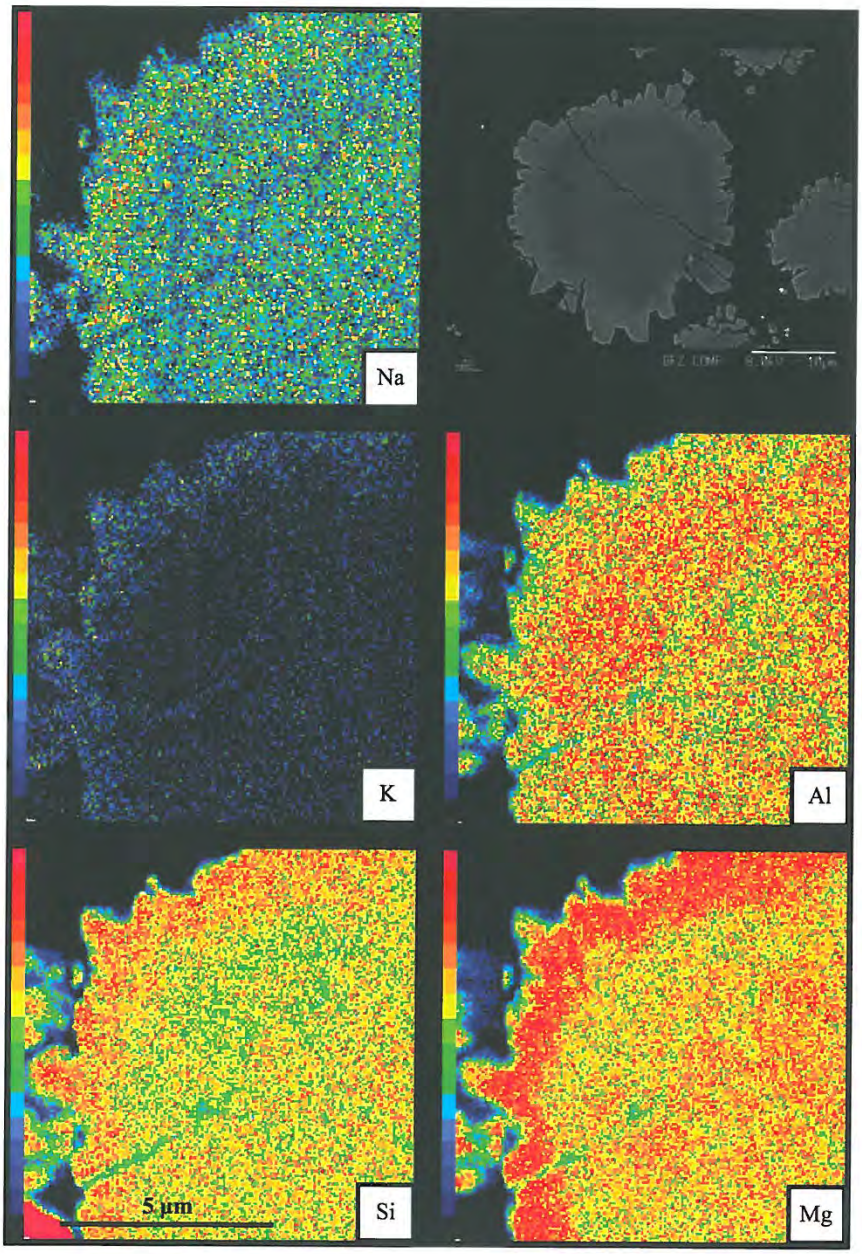

CROP: FIGURE 3

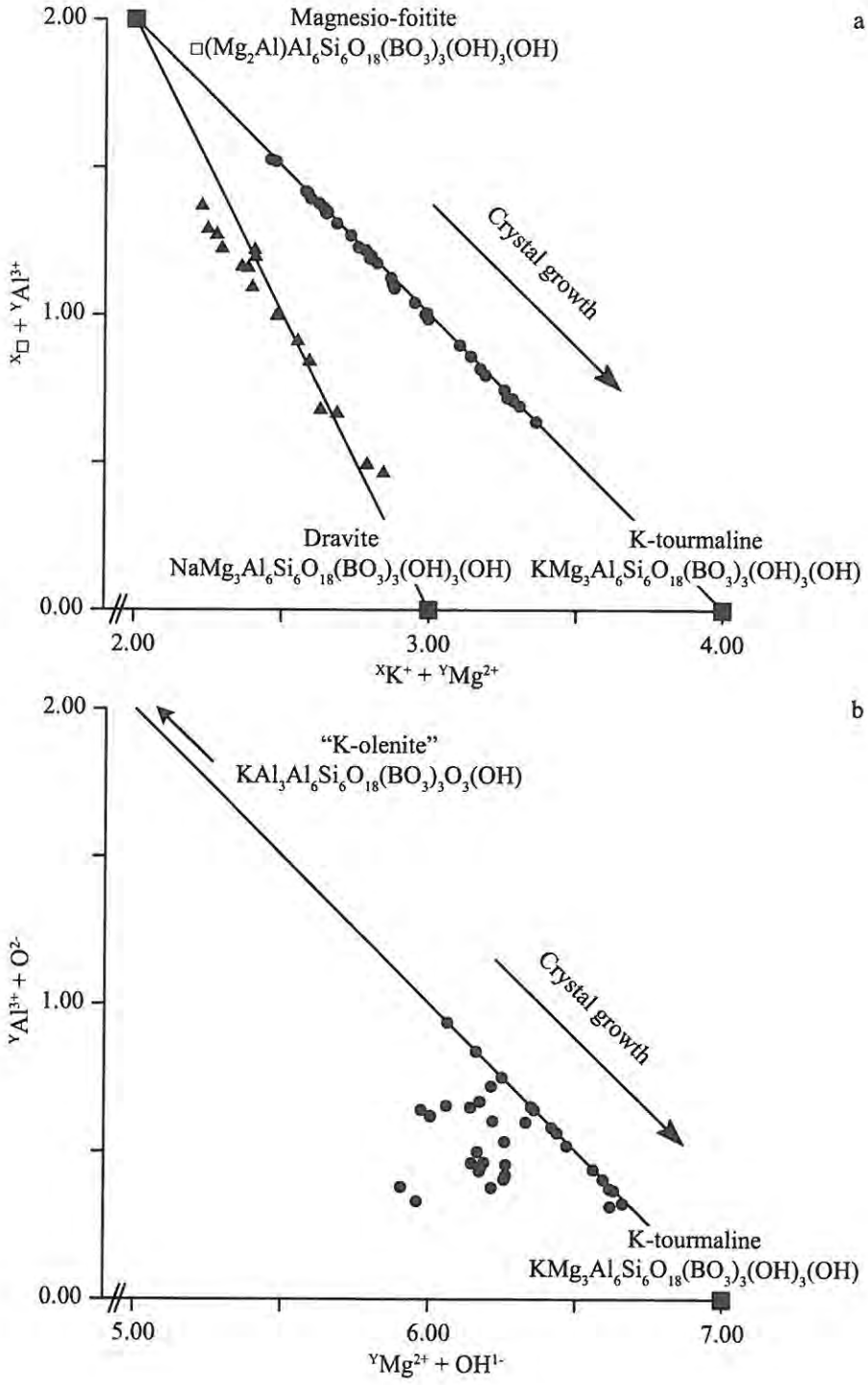

This is a preprint, the final version is subject to change, of the American Mineralogist (MSA)
Cite as Authors (Year) Title. American Mineralogist, in press.
(DOI will not work until issue is live.) DOI: http://dx.doi.org/10.2138/am.2014.4775 

CROP: FIGURE 4